Available online at www.sciencedirect.com
SCIENCE DIRECT
Journal of Power Sources 145 (2005) 178–187
JOURNAL OF POWER SOURCES
www.elsevier.com/locate/jpowsour

The influence of carbon support porosity on the activity of PtRu/Sibunit anode catalysts for methanol oxidation

V. Rao [a], P.A. Simonov [b], E.R. Savinova [a,b,*], G.V. Plaksin [c], S.V. Cherepanova [b], G.N. Kryukova [b], U. Stimming [a]

[a] *Technische Universität München, Physik-Department E19, James-Franck Str. 1, D-85748 Garching, Germany*
[b] *Boreskov Institute of Catalysis, Russian Academy of Sciences, Pr. Akademika Lavrentieva 5, 630090 Novosibirsk, Russia*
[c] *Institute for Problems of Hydrocarbon Processing, Neftezavodskaya st. 54, 644040 Omsk, Russia*

Accepted 29 December 2004
Available online 3 May 2005

Abstract

In this paper we analyse the promises of homemade carbon materials of Sibunit family prepared through pyrolysis of natural gases on carbon black surfaces as supports for the anode catalysts of direct methanol fuel cells. Specific surface area (S_{BET}) of the support is varied in the wide range from 6 to 415 $m^2\,g^{-1}$ and the implications on the electrocatalytic activity are scrutinized. Sibunit supported PtRu (1:1) catalysts are prepared via chemical route and the preparation conditions are adjusted in such a way that the particle size is constant within ±1 nm in order to separate the influence of support on the (i) catalyst preparation and (ii) fuel cell performance. Comparison of the metal surface area measured by gas phase CO chemisorption and electrochemical CO stripping indicates close to 100% utilisation of nanoparticle surfaces for catalysts supported on low (22–72 $m^2\,g^{-1}$) surface area Sibunit carbons. Mass activity and specific activity of PtRu anode catalysts change dramatically with S_{BET} of the support, increasing with the decrease of the latter. 10%PtRu catalyst supported on Sibunit with specific surface area of 72 $m^2\,g^{-1}$ shows mass specific activity exceeding that of commercial 20%PtRu/Vulcan XC-72 by nearly a factor of 3.

Keywords: Carbon support; Sibunit carbons; PtRu anode; DMFC; Catalyst utilisation; Anode performance

1. Introduction

Direct methanol fuel cells (DMFCs) using polymer electrolyte membranes are presently being considered candidate power sources for portable power and electric vehicle applications. Capability of DMFCs to consume liquid fuels without reformation is a serious advantage, since liquid fuels provide high specific energy and are easy to handle. DMFCs can be used as power sources in a few mW to several kW power range. There have been successful commercialisation efforts for DMFCs, smart fuel cells [1] being the first to introduce them into the market for portables, camping equipment, etc. Unfortunately, DMFCs are still very expensive, which puts a hurdle on the large-scale commercialisation of this promising technology. High costs of DMFCs come from expensive Nafion® membranes on the one hand, and high noble metal loadings, necessary to sustain reasonable power densities, on the other hand [2,3]. The latter are necessitated by sluggish anode and cathode kinetics, which limit the DMFC performance [2,4].

In DMFCs, methanol is electrooxidised at the anode to CO_2, resulting in electric current. Electrocatalysts having higher activity for methanol oxidation are critically needed to achieve an enhanced DMFC performance. Since up to now only platinum is known to have the ability to activate and break C–H bonds in the temperature range of DMFCs (from 25 to 130 °C), all presently available anode catalysts contain significant amounts of Pt [2,4–8]. Because of the high costs and low availability of Pt, there have been considerable efforts

* Corresponding author. Present address: Boreskov Institute of Catalysis, Russian Academy of Sciences, Pr. Akademika Lavrentieva 5, 630090 Novosibirsk, Russia.
E-mail address: elensav@catalysis.ru (E.R. Savinova).

0378-7753/$ – see front matter © 2005 Elsevier B.V. All rights reserved.
doi:10.1016/j.jpowsour.2004.12.064

to extract maximum performance from minimum amount of this noble metal. Introduction of catalysts dispersed on electrically conducting and high surface area carbon materials [2,4,9,10] was a significant step forward, which resulted in finer dispersion of the metal catalyst and thus higher electrochemically active surface area.

Different carbons have been tested as catalyst supports for fuel cell applications. Carbons with high specific surface areas (like Ketjenblack) are beneficial in terms of providing high dispersion of the active component, other conditions being equal. On the other hand, utilisation of high surface area carbons as supports for fuel cell electrocatalysts may result in Ohmic and mass transport limitations. Hence, Vulcan carbons with specific surface areas around 200 $m^2\,g^{-1}$ are often used as a reasonable compromise. However, to our knowledge, optimal properties of Vulcan carbons for either PEMFC (polymer electrolyte fuel cell), or DMFC applications have not been verified experimentally.

Many research groups have recently made efforts to unravel the influence of carbon support properties on the activity of fuel cell electrocatalysts. Uchida et al. [11,12] have found that metal nanoparticles residing in carbon pores below 40 nm in diameter, have no access to Nafion® ionomer and thus do not contribute to the electrochemical activity. This decreases the extent of catalyst utilisation denoted as a ratio of the electrochemically accessible surface area of metal nanoparticles to their total surface area. In order to improve the extent of metal–ionomer interaction, Uchida et al. [11,12] experimented with specific surface areas of acetylene black carbons. They reported on a decreased internal resistance of the catalyst layer and an improved PEMFC performance relative to conventional carbon supported catalysts, because of better Nafion®-catalyst contact.

Electrocatalysts consisting of platinum particles supported on graphite nanofibers (GNF) were prepared by Bessel et al. [13], who reported a four-fold improvement of mass activities for methanol electrooxidation in sulphuric acid electrolyte. Lukehart's group [14–16] prepared a PtRu/herringbone GNF nanocomposite using a single-source molecular precursor as a metal source, and performance of a DMFC with this nanocomposite as the anode catalyst was enhanced by 50% relative to that recorded for an unsupported PtRu anode catalyst.

More recently nanotubes (single walled and multiple walled) [17–20], graphitic carbon nanofibres (GCNF), nanocoils, and many other proprietary carbons have been investigated to find an optimum carbon support for fuel cell applications [16]. Carbon nanocoils, as reported in Refs. [21–24], provide at least two times higher activity for methanol oxidation in comparison to Vulcan XC-72. The authors tentatively attributed the enhancement to higher crystallinity (and hence lower Ohmic resistance), higher surface area and appropriate porosity of these carbon materials. Takasu et al. [25] studied the influence of specific surface area of carbon supports on the size and extent of alloying of metal catalyst particles.

Carbon materials affect many vital properties of supported metal catalysts, in particular: (i) metal particle size, morphology and size distribution [26,27]; (ii) extent of alloying in bimetallic catalysts [25]; (iii) stability of supported metal nanoparticles towards particle growth and agglomeration; (iv) electrocatalytic activity, e.g. due to metal-support interactions; (v) degree of catalyst utilisation; (vi) mass transport in the catalytic layer; (vii) electronic conductivity of the catalyst layer and thus its Ohmic resistance, etc. [13,22]. Hence, we believe that optimisation of the carbon support is of *crucial importance* for the development of PEMFCs and DMFCs. On the other hand, versatile multiple influences of carbon supports on electrocatalytic properties and hence fuel cell performance, makes it difficult to understand its physical origin and puts a hurdle on catalyst optimisation. Thus, one and the same property of carbon may be advantageous at the stage of catalyst preparation, being detrimental at the stage of fuel cell operation. For example, carbon materials with high specific surface area (which usually originates from high contribution of micro- and mesopores) allows better metal dispersion at the catalyst preparation step, but may lead to Ohmic and mass transport limitations during fuel cell operation. That's why, despite considerable efforts, it is still not completely clear which carbon properties are beneficial for fuel cell applications.

In this paper we introduce an approach to systematically investigate the effect of carbon support porosity and specific surface area on the PtRu anode performance by decoupling between the influence of support on (i) the catalyst preparation and hence metal dispersion, and (ii) its operation in a DMFC.

2. The approach

In this work we explore a possibility to use carbons of Sibunit family as supports for preparing catalysts for low temperature fuel cells. These carbon materials are prepared through pyrolysis of natural gases on carbon black surfaces followed by activation to achieve desired values of the surface area and pore volume [28]. Pyrolysis leads to formation of dense graphite-like deposits. During the activation, at first, the carbon black component is burned off. Hence, the pore size distribution in the final Sibunit sample roughly reproduces the particle size distribution in the carbon black precursor. Thus, varying the type of the gas source, the template (carbon black), and the manner and duration of the activation, it is possible to produce meso- or macroporous carbon materials with surface areas from 1 to 50 (non-activated) to 50–500 $m^2\,g^{-1}$ (activated) and pore volume up to 1 $cm^3\,g^{-1}$. This gives a unique opportunity to vary the specific area of carbon supports, keeping their chemical nature essentially intact. Other advantages of carbons of the Sibunit family are: (i) purity, (ii) high electrical conductivity, and (iii) uniform morphology of primary carbon globules (contrary to carbon blacks, in particular Vulcan [29]).

The idea introduced in this work is to widely vary the specific surface area of the carbon support (from a few meters per gram to a few hundreds meters per gram), keeping the size and structure of the active PtRu component possibly constant. Electrocatalytic activity of PtRu nanoparticles has been found to be strongly influenced by the metal dispersion. Takasu et al. [30] have found that mass specific activity of PtRu nanoparticles in methanol oxidation (measured in H_2SO_4 electrolyte at 60 °C) passes through a maximum at ca. 3 nm and decreases markedly, as the particle size decreases. Keeping this in mind, in this work we aimed at keeping the size of PtRu particles close to 3 nm. However, the latter is hard to attain, if metal loading is kept constant, while specific surface area of carbon supports is varied in a wide range. Indeed, metal dispersion is known to decrease, if either (i) the specific surface area of a carbon support is reduced at a constant metal loading [25] or (ii) the amount of metal is raised at a constant support surface area [30,31]. Hence, Guerin et al. [32] reported that the average particle size of commercial Johnson Matthey Pt catalysts supported on Vulcan XC-72R increased from ca. 1 nm to ca. 6.5 nm, when the metal loading was raised from 10% to 78%. CO stripping voltammograms presented by the authors suggest that significant part of nanoparticles in high loading catalysts is agglomerated. In this work, in order to keep the particle size around 3 nm, we varied the amount of metal (PtRu) per unit mass of a carbon support. Thus, for the low surface area carbon supports (Sib_P2677 with 22 $m^2\,g^{-1}$ and Sib_19P with 70 $m^2\,g^{-1}$) the metal percentage was set at 10 wt.%, while for high surface area carbon supports (Sib_20P with 292 $m^2\,g^{-1}$ and Sib_619P with 415 $m^2\,g^{-1}$), it was increased to 20 wt.%. The catalyst supported on Sib_176K with 6 $m^2\,g^{-1}$ specific surface area, contained only 1%PtRu.

The thickness of the catalyst layer is another parameter, which plays an important role in the overall performance of a fuel cell. It affects Ohmic resistance, current and potential distribution and mass transport in the electrocatalyst layer [33–35]. Thus, differences in the intrinsic catalytic activities of two DMFC anode catalysts incorporated in MEAs with significantly different thicknesses of the catalyst layer may be overshadowed by the influence of mass transport. Therefore, in order to make a meaningful comparison between different catalysts, we kept the anode catalyst layer thickness constant by fixing the amount of the catalyst powder (metal + carbon) per cm^2 of the electrode geometrical area.

We believe that the approach introduced in this work offers a means of unveiling the influence of carbon support on the catalyst operation in an anode of a DMFC and will ultimately allow designing an optimum carbon supports for fuel cell applications.

3. Experimental

3.1. Catalyst preparation

Carbons of the Sibunit family (Omsk, Russia) with different specific surface areas ranging from 6 to 415 $m^2\,g^{-1}$ and Vulcan XC-72 (Cabot Corp.) were used as catalyst supports. PtRu (1:1) catalysts were prepared by co-hydrolysis of chloride complexes of Ru^{III} and Pt^{IV} using a procedure similar to that described by Reetz and Koch [36]. The authors of Ref. [36] found that an addition of alkali to a solution of $RuCl_3 + H_2PtCl_6$ results in the formation of small colloidal particles of mixed metal oxides, and added organic surfactants in order to prevent their further growth and coagulation. Unlike them, we avoided an addition of organic ligands (which form a shell around metal particles and may thus influence their activities in electrochemical processes), but performed synthesis in the presence of carbon supports, assuming that the latter may act as a macroligands stabilising colloids of mixed metal oxides. The preparation procedure comprised a number of steps schematically represented in Fig. 1.

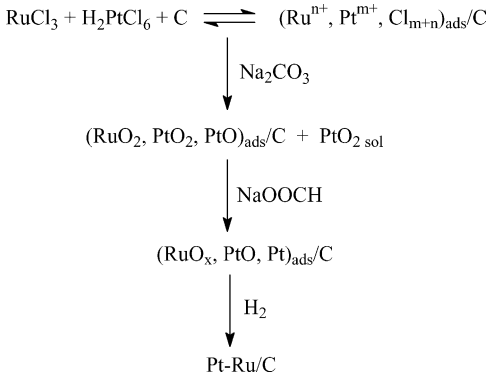

Fig. 1. Schematic representation of the catalyst synthesis.

3.2. Characterisation of the catalysts

Textural characteristics of carbon supports were obtained from the data on nitrogen adsorption measured at 77 K with an automatic volumetric analyzer ASAP 2400 (Micrometrics) and are given in Table 1. Carbon samples were pretreated at 573 K to residual pressure of ca. 10^{-3} Torr. The adsorption isotherms were used to calculate values of BET specific surface area S_{BET} (in the range $P/P_0 = 0.05$–0.2) and total pore volume V_Σ (at $P/P_0 = 0.98$). Here P_0 is the saturation pressure. The volume of micropores V_{mi} accessible to nitrogen at 77 K and the total surface area of meso- and macropores A_α were determined using comparative method introduced by Karnaukhov et al. [37]. The latter is analogous to α_s-method of Sing or *t*-method of Lippens–de Boer (see Ref. [37] and references therein). The volume *V* and the surface area *S* of the pores between 1.7 and 300 nm were calculated from the adsorption (BJH cum. ads.) and desorption (BJH cum. des.) branches of the capillary condensation hysteresis according to the BJH model [38]. Values of mesopore diameters *D* were calculated on the basis of the BET and BJH models as $D = 4V/S$. Pore size distributions were acquired using BJH cum. desorption method and represented in Fig. 2 for selected carbon samples.

Table 1
Textural characteristics of carbon materials

Textural characteristics[a]	Vulcan XC-72	Sib_176K	Sib_P2677	Sib_111P	Sib_19P	Sib_20P	Sib_619P
Surface area ($m^2\,g^{-1}$)							
S_{BET}	252	5.96	21.9	64.1	72.3	292	415
A_α	177	7.10	23.8	58.9	65.7	330	470
$S_{(BJH\ cum.\ ads.)}$	94	4.06	18.5	–	33.0	146	222
$S_{(BJH\ cum.\ des.)}$	103	4.10	22.1	38.2	46.9	239	351
Pore volume ($cm^3\,g^{-1}$)							
V_Σ	0.63	0.018	0.117	0.105	0.154	0.416	0.593
$V_{(BJH\ cum.\ ads.)}$	0.547	0.016	0.114	–	0.132	0.325	0.470
$V_{(BJH\ cum.\ des.)}$	0.550	0.016	0.116	0.088	0.138	0.373	0.532
V_{mi}	0.037	0.000	0.000	0.0024	0.004	−0.012[b]	−0.019[b]
Pore size (nm)							
$D_{(by\ BET)}$	7.5	11.8	21.4	6.5	8.5	5.7	5.7
$D_{(by\ BJH\ cum.\ ads.)}$	23.3	16.0	24.7	–	16.0	8.9	8.5
$D_{(by\ BJH\ cum.\ des.)}$	21.3	15.9	21.0	9.2	11.8	6.2	6.0

[a] See Section 3.2 for details.
[b] Since V_{mi} is determined as an intercept of the t-plot, its negative values do not have physical meaning and point to the absence of micropores.

The X-ray diffraction (XRD) patterns of PtRu/C catalysts were obtained using X-ray diffractometer (Siemens, Cu Kα radiation) featuring a high-temperature camera-reactor [39]. A catalyst sample stored under ambient conditions was re-reduced in H_2 flow at 150 °C for 1 h, then cooled down to room temperature, and then its X-ray diffraction pattern was recorded by scanning in the 2Θ angle range from 20° to 100°. Calculation of the lattice parameter and the average size of metallic crystallites were based on the angle position, and on the half-width of the 111 diffraction line for fcc structure, respectively.

Pulse CO chemisorption experiments were performed with powder PtRu/C samples in H_2 atmosphere at 20 °C. These were used for calculating metal dispersion, assuming that each Pt and Ru surface atom adsorbs one CO molecule.

Metal particle size distributions (PSD) were obtained from transmission electron microscopy (TEM) images (JEM-2010 microscope) and used to calculate average

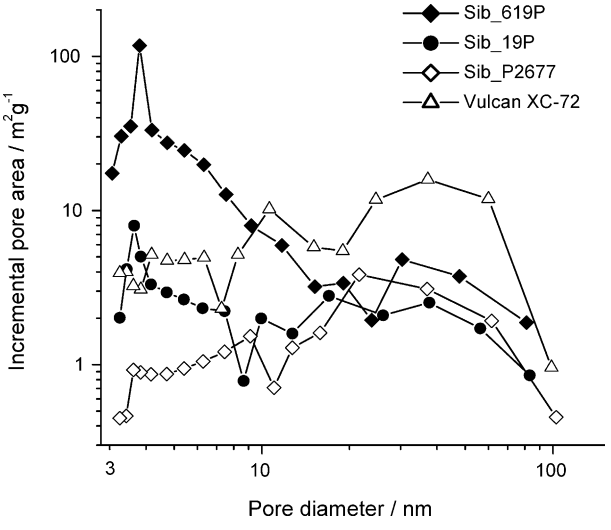

Fig. 2. Pore size distributions from BJH desorption method.

$\overline{d} = \frac{\sum_i n_i d_i}{\sum_i n_i}$, number-average $d_n = \frac{\sum_i n_i d_i^2}{\sum_i n_i d_i}$, surface-average $d_s = \frac{\sum_i n_i d_i^3}{\sum_i n_i d_i^2}$, and mass-average $d_m = \frac{\sum_i n_i d_i^4}{\sum_i n_i d_i^3}$ diameters of metal particles.

3.3. Preparation of membrane electrode assemblies (MEAs)

Homemade PtRu (1:1) catalysts supported on Sibunit carbons and on Vulcan XC-72, as well as commercial 20%PtRu(1:1)/Vulcan XC-72 catalyst from E-TEK, were used for the preparation of the anode. Pt/Vulcan (40 wt.%, E-TEK, Alpha Aesar) was utilised as the cathode catalyst. In order to make a MEA, a suspension of the catalyst powder, Nafion® solution (Dupont), and isopropanol were treated in an ultrasonicator. The ink was sprayed onto porous carbon backing layers (Toray paper from E-TEK, TGPH 060, no wet proofing), held at 110 °C. The 1.2 cm^2 patches of the Toray paper comprising sprayed catalyst layers were then cut and hot pressed with the Nafion® 117 membrane in between at 140 °C for 5 min at a pressure of 826 Ncm^{-2}. In order to keep the thickness of the anode electrocatalyst layer constant, we kept the amount of the catalyst powder (metal + carbon) around 1.5 mg cm^{-2} for all carbon supports.

3.4. Electrochemical measurements

The DMFC consisted of two stainless steel plates with integrated serpentine medium distribution channels. The DMFC was operated at 50 °C in a half-cell mode in order to have a control of the anode potential. The anode compartment was fed with 1 M aqueous methanol solution with a flow rate of 5 $cm^3\,min^{-1}$ and the cathode was purged with pure H_2 supplied with a flow rate of 20 $cm^3\,min^{-1}$ (controlled by a MKS flow meter). A dosing pump between the cell outlet and the exit tank controlled the flow of the methanol solution

and water through the cell. The methanol solution and the Millipore water (18.2 MΩ cm) were deaerated with argon. To avoid gas bubble formation due to large CO_2 production and its low solubility at elevated temperature, the anode flow system was pressurised at 3 bar overpressure. The cathode overpressure was kept at 1 bar to limit crossover of H_2 to the anode side. The cathode potential was assumed equal to the potential of the reversible hydrogen electrode (RHE). All potentials reported are in reference to this electrode. Special experiments were performed, which proved that methanol penetration into the reference electrode compartment did not influence the value and the stability of its potential. No correction for the IR drop was made. The anode flow system comprised a tank filled with methanol solution and a tank filled with water. These tanks were connected via heated tubes with the three-way valve at the DMFC inlet. A potentiostat designed by AGEF was used together with computerised data acquisition system to record data.

After installing a MEA in a DMFC, cyclic voltammograms (CV) recorded in the interval between 0.03 and 0.8 V in a water flow exhibited double layer splitting, but no clear adsorption/desorption peaks were observed. During conditioning of the catalyst at 90 °C, anodic and cathodic peaks gradually developed at ca. 100 mV versus RHE (see Fig. 5) and after approximately 8 h a stable CV was attained. Only after such a conditioning, the *I–U* curves and CO stripping voltammograms were recorded. The *I–U* curves for methanol oxidation were measured at a sweep rate of 0.5 mV s^{-1}. No hysteresis between the anodic and the cathodic sweep was observed at this slow sweep rate.

4. Results and discussion

4.1. Catalyst characterization

Data presented in Table 1 indicate that unlike Vulcan XC-72, Sibunit carbons do not contain micropores (see V_{mi}). This is also reflected in the close values of A_α and S_{BET} for Sibunit carbons, while for Vulcan XC-72 A_α is significantly lower than S_{BET}. Pores sized between ca. 1 and 2 nm give noticeable contribution to the surface area of high surface area Sibunit carbons (samples 619P and 20P) as well as of Vulcan XC-72, as indicated by the difference between A_α and S_{BJH} values. Fig. 2 shows that the decrease of the specific surface area of Sibunit carbons from samples 619P to 20P, 19P and finally P2677 occurs at the expense of pores below 20 nm size, whose contribution drops, while the average contribution of macropores above 20 nm stays essentially unchanged. This is reflected also in an increase of the average pore size and a decrease in the pore volume (Table 1).

CO chemisorption points to high metal dispersion in all PtRu/C catalysts under study, its values varying between 0.24 and 0.46 (Table 2). TEM images of selected catalysts shown in Fig. 3a and b evidence that PtRu nanoparticles are separated and uniformly distributed on support surfaces. Fig. 3b also demonstrates "shell" morphology of high surface area Sibunit carbons, which results from the total burn-off of primary carbon black globules during their steam activation. Narrow particle size distributions are observed for catalysts supported on high as well as on low surface area Sibunit carbons (see inserts to Fig. 3a and b). This is demonstrated also by close $\overline{d}$, d_s and d_m values (Table 2). On the contrary, PtRu particles supported on Vulcan XC-72 show bimodal particle size distribution, likely originating from the inhomogeneity of the support. Examination of extended support areas proved that predominant part of metal particles on Sibunit supports is not agglomerated.

Table 2
Dispersion and average metal particle size in PtRu/C catalysts

Catalyst	Dispersion	Mean particle size (nm)				
	CO/M	$d_{chem.}$	$\overline{d}$	d_n	d_s	d_m
1%PtRu/Sib_176K	0.42	2.4	1.8	1.9	1.9	1.9
10%PtRu/Sib_P2677	0.32	3.2	3.3	3.5	3.6	3.8
10%PtRu/Sib_19P	0.36	2.8	2.6	2.8	3.0	3.1
20%PtRu/Vulcan XC-72[a]	0.40	2.5				
20%PtRu/Sib_19P	0.24	4.2	3.7	3.8	3.9	4.1
20%PtRu/Sib_20P	0.42	2.4				
20%PtRu/Sib_619P	0.46	2.2	2.0	2.1	2.1	2.2

[a] Non-uniform PtRu distribution: particles of 15–25 Å in diameter are predominantly observed, while some areas of the support surface are covered with large particles ca. 50 Å size.

Comparison of CO chemisorption and TEM data suggests that metal dispersion (CO/M) and surface-average size of the particles (d_s) obey the equation:

$$d_s(nm) \approx \frac{1}{\mathrm{CO/M}} \quad (1)$$

Numerical coefficient in this equation is somewhat higher than the one reported for pure ruthenium catalysts (d_s = 0.91/(CO/Ru) [40], but lower than for platinum (d_s = 1.08/(CO/Pt) [41]. Using chemisorption data and Eq. (1), we estimated the average particle size d_{chem} for PtRu/C catalysts (Table 2). One may see that the preparation procedure employed in this study allows keeping the average particle within 2.2 and 4.2 nm despite considerable variation (by a factor of 70) of S_{BET} of carbon supports.

XRD measurements were performed in air and in H_2-filled XRD chamber. Fig. 4a compares XRD patterns acquired for 20%PtRu/Sib_619P sample stored in air and after its reduction in the XRD chamber. The former hardly shows any metal reflections, indicating that PtRu particles are grossly oxidised under ambient atmosphere. The extent of metal oxidation depends critically on the dispersion of the metal particles, increasing with the increase of the latter. Oxidation of supported PtRu particles under ambient conditions has been reported earlier [14,16,42,43]. As evidenced by Fig. 4a, treatment of the catalyst sample in hydrogen atmosphere at 150 °C, results in its reduction and formation of metallic PtRu particles. XRD patterns of reduced sample represented in Fig. 4b do not show

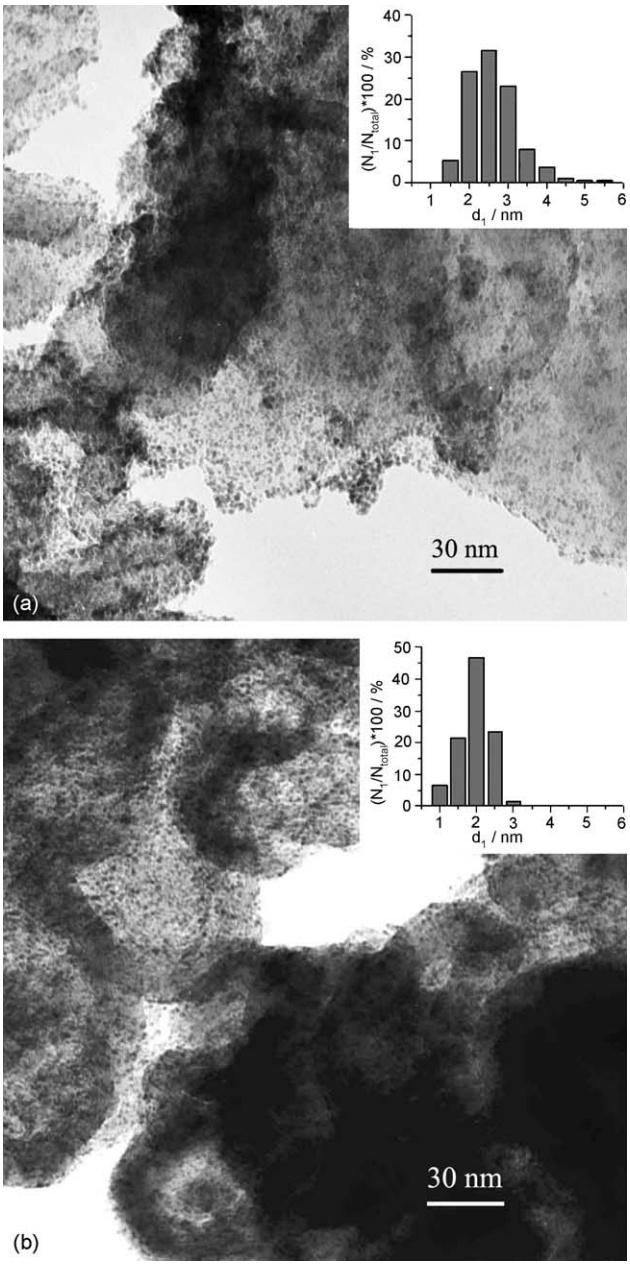

Fig. 3. TEM images and particle size distributions for (a) PtRu/Sib_111P (S_{BET} = 64.1 $m^2\ g^{-1}$) and (b) PtRu/Sib_619P (S_{BET} = 415 $m^2\ g^{-1}$). Particle size distributions are shown in the insets.

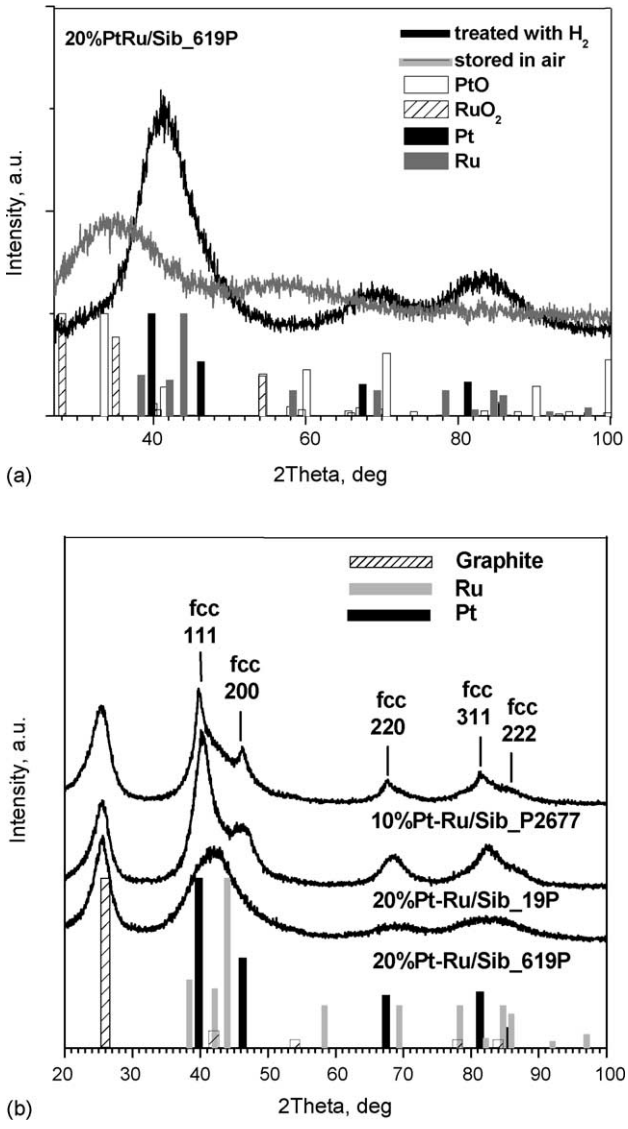

Fig. 4. XRD patterns for PtRu/Sibunit catalysts: (a) 20%PtRu/Sib_619P stored in air and reduced in H_2 after subtraction of the diffraction from the support; (b) 10%PtRu/Sib_P2677; 20%PtRu/Sib_19P and 20%PtRu/Sib_619P reduced in H_2. Bars show positions and intensities of the reflections corresponding to graphite, metallic Pt, Ru and their oxides.

either (1 0 1) or (1 0 2) Ru reflections at $2\theta = 44$ and 58.3°, respectively. This confirms that Ru is not segregated in a separate phase and most of the metal is comprised in bimetallic alloy nanoparticles. Previously, it has been reported that interaction of oxygen with alloy RuPt or RuPd particles depletes them from Ru due to formation of ruthenium oxide phases. In the course the catalyst reduction with hydrogen, three scenarios have been observed: (i) Ru segregates into a separate phase and forms monometallic nanoparticles, (ii) Ru metal is segregated onto the surfaces of alloy particles [44], or (iii) bimetallic RuM alloy particles are formed [45]. In our case, obviously the latter scenario is realised, with reduction giving rise to alloy PtRu particles. This is confirmed both by the absence of separate reflections from Ru phase and by the value of the lattice parameter, which is equal to 3.88 Å for 20%PtRu/Sib_19P and 3.90 Å for 10%PtRu/Sib_2677P. It should be pointed out, however, that precise determination of diffraction line positions in this work is not feasible due to the (i) high metal dispersion, which stipulates line broadening and an overlap of (1 1 1) and (2 0 0) reflections from fcc PtRu nanoparticles, and (ii) superposition of (0 0 2) reflection from carbon support with metal reflexes. 20%PtRu/Sib_619P catalyst represents the most dramatic example, where due to the high metal dispersion (1 1 1) and (2 0 0) reflections merge together.

Table 3
Influence of the Nafion® content on the mass activity[a] at 0.5 V vs. RHE

Catalyst sample	Nafion® content (wt.%)				
	13	17	23	29	34
10%PtRu/Sib_P2677		268	190		29
10%PtRu /Sib_19P		272	257		
20%PtRu/Sib_19P	178	174			
20%PtRu/Vulcan XC-72		110		101	
20%PtRu/Sib_20P		130		119	

[a] Mass activity is given in $A g^{-1}$ at 50 °C and 1 M methanol feed, with DMFC in a half cell mode.

4.2. Optimisation of the Nafion® content in MEAs

It has previously been reported that fuel cell performance may be noticeably influenced by the ionomer content in the catalyst layer [46–48]. Since specific surface areas of carbon supports utilised in this study are grossly different, a priori it was not clear which amount of Nafion® ionomer was necessary to ensure high intra-layer ionic conductivity and optimum catalyst performance for each of these supports. Hence, in order to compare the catalyst performance under optimised conditions, the amount of ionomer in the catalyst layer was varied for each carbon support. The results are given in Table 3. Despite our expectations, the influence of ionomer content on the activity of PtRu/Sibunit catalysts in methanol oxidation is not very pronounced. Only at a very high (34%) Nafion® content the activity of 10% PtRu/Sib_P2677 sample dropped noticeably, supposedly due to blocking metal particles and hindering methanol diffusion to and CO_2 diffusion from their surfaces. The optimum amount of ionomer was close to 17 wt.% of dry Nafion® in the anode layer for all the catalysts explored and was further on used for all MEA preparations. An independence of the optimum Nafion® content on S_{BET} in a wide interval from 22 to 416 $m^2 g^{-1}$ can be explained by pore size distributions in Sibunit carbons (Fig. 2). As mentioned above, an increase of Sibunit surface area occurs mainly due to an increase of the amount of pores below 20 nm in size. Since according to Uchida et al. [11,12], Nafion® micelles penetrate mainly in macropores (>40 nm diameter), smaller pores, which develop upon an increase of the surface area of Sibunit carbons, do not demand more Nafion®.

Arico et al. [48] have also observed little influence of Nafion® content in the Vulcan XC-72 supported PtRu anode catalyst layer on the performance of DMFCs. They have found ca. 15% increase in the cell performance, when the amount of Nafion® was raised from 15 to 33%. Meanwhile, our experiments reveal 10% decrease in the mass activity, when Nafion® content increased from 17 to 29% (Table 3). It should be noted that the optimum Nafion® amount may depend on the carbon support structure, the metal loading, etc. Thus, Sasikumar et al. [47] observed an increase in the optimum Nafion® content for a PEMFC from 20 to 40 and then 50 wt.% upon a decrease of the platinum loading from 0.5 to 0.25 and then 0.1 mg(Pt)cm^{-2}, respectively.

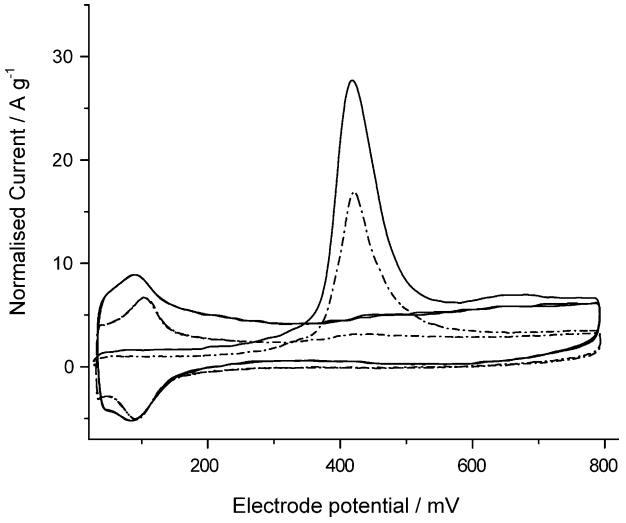

Fig. 5. Typical CO stripping voltammograms at 50 °C and 5 mV s^{-1} scan rate, measured in a half-cell DMFC. *Y*-axis shows the current normalised to metal loading. Solid line corresponds to 10%PtRu/Sib_P2677 and dotted line to 20%PtRu/Vulcan XC-72.

4.3. Metal utilisation in PtRu/C electrocatalysts

Metal utilisation α in electrocatalysts is calculated as a ratio of the electrochemically active surface area (EASA) and the total metal surface area (TSA). The latter is derived from the amount of CO chemisorbed from the gas phase (N_{CO}^{Chem}), while the former is determined from the amount of electrochemically stripped CO (N_{CO}^{Chem}). Finally, α is calculated using the formula:

$$\alpha = \frac{\text{EASA}}{\text{TSA}} = \frac{N_{CO}^{Echem}}{N_{CO}^{Chem}} = \frac{Q}{2FN_{CO}^{Chem}}$$

Here Q is the CO stripping charge and F is the Faraday constant.

Typical CO stripping votammograms are shown in Fig. 5 for 10%PtRu/Sib_P2677 and for 20%PtRu/Vulcan XC-72 catalysts. The stripping charge Q is calculated as the area under CO stripping peak versus the background (second scan) in 0.35–0.8 V potential range. EASA is then calculated assuming 385 μC cm^{-2} [50].

In Fig. 6, α is plotted versus S_{BET} of carbon supports. The figure clearly shows that the catalyst utilisation factor rises along with the decrease of S_{BET}. For PtRu/Vulcan XC-72 (S_{BET} = 252 $m^2 g^{-1}$), α amounts to 50–55%, which agrees well with the data reported in the literature [51,52]. For Sibunit 19P (S_{BET} = 72 $m^2 g^{-1}$) α exceeds 1, which may be either due to the experimental uncertainty, or to a systematic error arising from an overestimation of CO stripping charge Q. Thus, according to Jusys et al. [53], contribution of the double layer charge to Q for PtRu surfaces may amount to 50%. If this is really so, values of α calculated in this work will be systematically overestimated for all the catalyst samples. This, however, will not change the observed trend of the increase of α with S_{BET}.

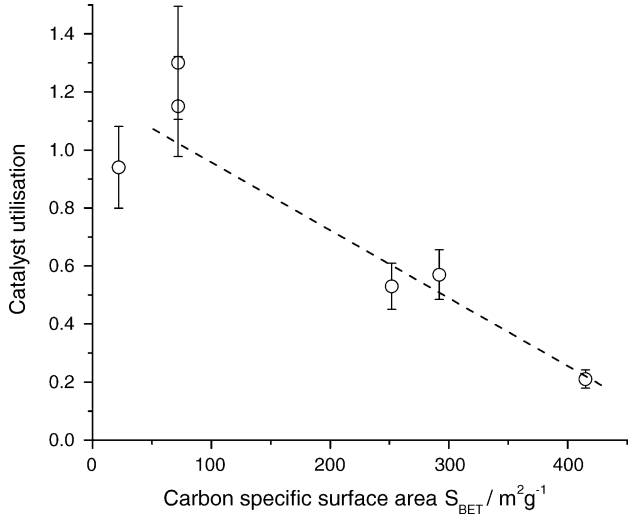

Fig. 6. Catalyst utilisation factors plotted vs. S_{BET} of carbon supports.

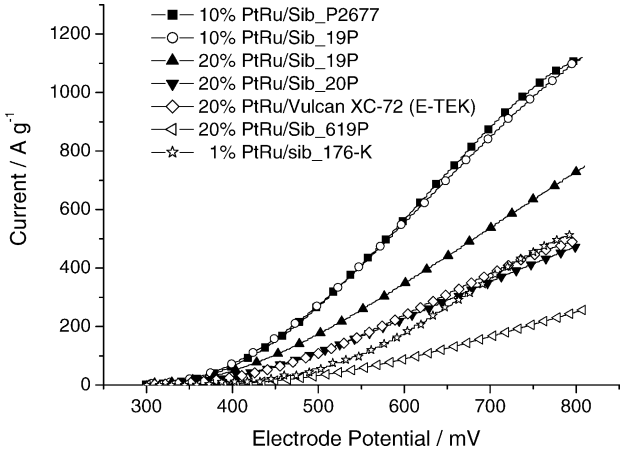

Fig. 7. Current–potential characteristics for PtRu anode catalysts at 50 °C and 0.5 mV s^{-1} scan rate, measured in a half-cell DMFC. *Y*-axis shows current normalised to the metal loading.

The trend of decreasing metal utilisation with an increasing support surface area can be explained on the basis of an increased incompatibility between the morphological structure of carbon support and Nafion® micelles. In CO chemisorption all the metal sites, which are exposed to the surface of nanoparticles and adsorb CO, are counted, since CO gas can reach every nanoparticle regardless its location (unless its surface is blocked by the pore walls or carbonaceous deposits [27]. However, this is not the case in an electrochemical CO stripping experiment from a PtRu/C catalyst incorporated in a MEA. The latter provides information only on the amount of PtRu sites, which are in contact with the Nafion® ionomer and thus can participate in the electrochemical process. As the surface area of carbon supports increases, more small pores with $d < 20$ nm are formed (Fig. 2). Meanwhile, according to Refs. [12,49], Nafion® ionomer has rather large (>40 nm) micelles, which do not penetrate in carbon pores of smaller diameter. The results of this work strongly suggest that an increase of the contribution of pores with $d < 20$ nm results in a considerable decrease of the metal utilisation factor (cf. Figs. 6 and 2), thus providing a qualitative proof for the data reported by Uchida et al. [12]. Thus, low surface area carbon materials, featuring minimum (if at all) contribution of pores below 20 nm, favour high catalyst utilisation in MEAs of fuel cells with polymer electrolytes.

4.4. Methanol oxidation

Fig. 7 shows current potential characteristics for PtRu catalysts supported on Sibunit and on Vulcan XC-72 in 1 M methanol. The most remarkable observation is that the catalysts supported on low surface area carbons (Sib_19P with $S_{BET} = 72\ m^2\ g^{-1}$ and Sib_P2677 with $S_{BET} = 22\ m^2\ g^{-1}$) show much superior mass activities. Vulcan XC-72 based catalysts (both homemade as well as commercial) show much lower mass activities. PtRu/Sib_619P catalyst, which support has very high surface area of $415\ m^2\ g^{-1}$ reveals the poorest performance. Surprisingly, the *I–U* curve for the 1%PtRu/Sib_176K catalyst with an extremely low carbon surface area of only $6\ m^2\ g^{-1}$ and low metal content lies much above that for 20%PtRu/Sib_619P and at high overpotentials approaches that for 20%PtRu/Vulcan XC-72 catalysts. Although high overpotential interval is of limited interest for fuel cell applications, the behaviour demonstrated by carbon material, containing grains with essentially geometric surface area (nearly no porosity) is interesting and deserves further exploration. The difference in mass activities between 10 and 20% catalyst supported on Sib_19P may be tentatively ascribed to different dispersions of PtRu particles (Table 2).

Mass activities of the catalysts at 0.5 V are plotted in Fig. 8 and show clear dependence on the S_{BET} of carbon supports. Mass activities increase systematically, as S_{BET} is reduced from 415 to $72\ m^2\ g^{-1}$. Sib_19P and Sib_P2677 supported samples demonstrate the highest mass activities, which are nearly three times higher compared to Vulcan XC-72. It

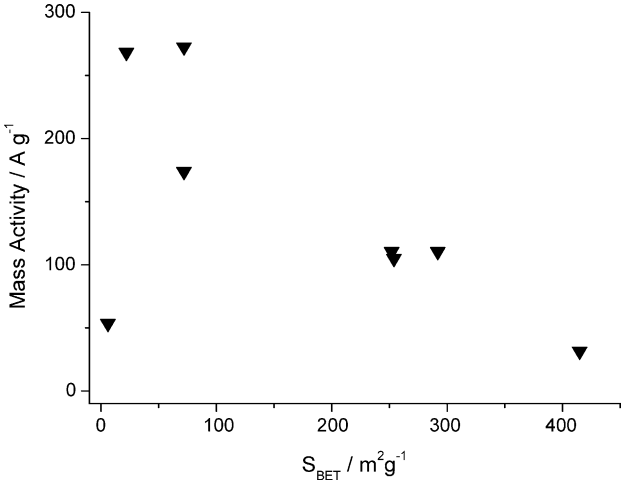

Fig. 8. Mass activities at 0.5 V RHE plotted vs. S_{BET} of carbon supports.

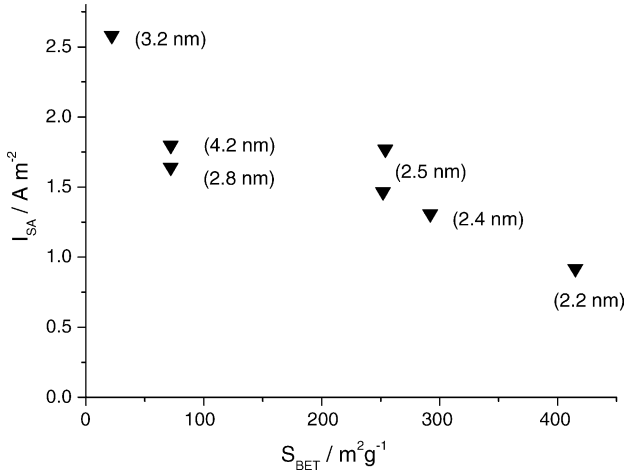

Fig. 9. Specific activities (A m^{-2}) at 0.5 V RHE plotted vs. S_{BET} of carbon supports. Unfortunately, due to experimental problems, data on EASA and hence specific activity of Sib_176K (6 m^2 g^{-1}) are not available.

should be stressed that this effect indeed arises from different pore structures of carbon materials, rather than from (i) different catalyst preparation procedures or (ii) different metal particle dispersions. Indeed, Table 2 proves that metal dispersions for 20%PtRu/Vulcan XC-72 and 10%PtRu/Sib_19P are very similar (0.4 and 0.36, respectively), while the difference in mass activities amounts to a factor of 3. The preparation procedure cannot explain the observed current enhancement either, as illustrated by the observed coincidence of the *I–U* curves for the commercial catalyst and the homemade 20%PtRu/Sib_20P, the latter having very similar to Vulcan XC-72 specific surface area (292 m^2 g^{-1}). The reason of low mass activity of the catalyst supported on Sib_176K with S_{BET} = 6 m^2 g^{-1} is not quite clear yet. Either catalytic activity has an optimum at S_{BET} between 20 and 70 m^2 g^{-1}, or the observed decrease of the catalytic activity results from the low (1 wt.%) metal content in the sample. At such a low metal content even small amounts of impurities in the catalyst layer may be detrimental for the catalytic activity.

Superior performance of low surface area carbons with S_{BET} between 20 and 70 m^2 g^{-1} was not unexpected, since we believe that utilisation of high surface area supports in PEMFCs and DMFCs leads to two disadvantages: (i) low metal utilisation and (ii) diffusion hindrance in narrow pores. While the influence of the metal utilisation on the catalyst performance is illustrated by Fig. 6 and was discussed above, the issue of diffusion hindrance in the pores needs further clarification. Therefore, we normalise anodic currents to EASA and obtain specific activity values (A m^{-2}), which are plotted in Fig. 9 for the anode potential of 0.5 V versus S_{BET}. If the differences in the metal utilisation were the only reason for the observed mass activity enhancement, the values of specific catalyst activities per unit of EASA should have been independent of S_{BET}. On the contrary, a clear trend of specific activity enhancement is observed, when carbon surface area is reduced from 415 to 22 m^2 g^{-1}.

Since despite our efforts, metal dispersion in the catalysts under study was not exactly the same, let us analyse whether the differences in specific activities might originate from different PtRu dispersions. For clarity, we indicate the average PtRu particle sizes measured by gas phase CO chemisorption in Fig. 9. Obviously, the differences observed cannot be attributed to the influence of the dispersion alone. As mentioned in the introduction, Takasu et al. [30] reported remarkable size effect for Vulcan XC-72 supported PtRu nanoparticles during methanol oxidation. They have observed a considerable decrease of the specific activity per unit surface area, when the average particle size decreased below 3 nm. In our case, size effects are obviously much less pronounced as illustrated by the close values of specific activities for 2.8 and 4.2 nm PtRu particles supported on Sib_19P. One should bear in mind, however, that Takasu et al. tested their catalysts in sulphuric acid, and not incorporated in MEAs with a polymer electrolyte, as in this work.

Comparison of Figs. 9 and 2 demonstrates clear correlation between the values of specific activity of PtRu methanol oxidation catalysts and the contribution of pores with $d < 20$ nm: the higher their contribution, the lower the activity. Indeed, Sib_P2677, which shows superior specific activity, features a very small amount of pores with $d < 20$ nm (Fig. 2). As S_{BET} increases, the contribution of the pores below 20 nm to the support surface area gradually increases, while the specific activity decays. Hence, the results of this work give evidence on the detrimental effect of pores with $d < 20$ on the specific activity of PtRu/C electrocatalysts in methanol oxidation. Diffusion hindrance inside small pores appears to be a likely reason for the observed phenomenon. It is not quite clear yet either this is due to slow methanol (or its oxidation products) diffusion or due to blocking the pore mouths by Nafion® micelles.

5. Conclusions and outlook

In this paper we introduce an approach to investigate the influence of specific surface area of carbon supports on the performance of the DMFC anode catalysts by keeping PtRu dispersion constant.

We utilise novel catalysts for an anode of a DMFC: PtRu nanoparticles supported on Sibunit carbons. Specific surface areas of carbon materials are varied systematically in a wide range from 6 to 415 m^2 g^{-1}. Low surface area carbon supported catalysts show superior mass specific activities, exceeding that of commercial 20%PtRu catalyst by nearly a factor of 3. The catalyst utilisation for low surface area carbons is close to 100%, which may be explained by the compatibility between the size of the pores in carbon supports and Nafion® micelles. Superior mass activity of low surface area carbon supports is attributed to (i) high PtRu surface utilisation, and (ii) facilitated diffusion in macropores.

This work is only a step on the way to design optimised supports for PEMFCs and DMFCs. However, it shows

immense potentialities of support optimisation in the improvement of low temperature fuel cell electrocatalysts. More work is needed in order to find out the (i) optimum pore structure and (ii) texture of carbon supports and to explore how surface area influences long term stability of fuel cell catalysts.

Acknowledgements

We thank DFG for financial support under contracts No. Sti 74-8-4 and 436RUS113-718-1-1 and V.I. Zaikovskii for his kind assistance with TEM measurements.

References

[1] http://www.smartfuelcell.de/.
[2] W. Vielstich, A. Lamm, H.A. Gasteiger (Eds.), Handbook of Fuel Cells, vol. 1, John Wiley & Sons, 2002.
[3] L. Carrette, K.A. Friedrich, U. Stimming, CHEMPHYSCHEM 1 (2000) 162.
[4] M.P. Hogarth, G.A. Hards, Platinum Met. Rev. 40 (1996) 150.
[5] A. Hamnett, Catal. Today 38 (1997) 445.
[6] H.A. Gasteiger, N. Markovic, P.N. Ross, E.J. Cairns, J. Electrochem. Soc. 141 (1994) 1795.
[7] M.P. Hogarth, P.A. Christensen, A. Hamnett, Proceedings of the First International Symposium on New Materials for Fuel Cell Systems, Montreal, July 9–13, 1995.
[8] P.A. Christensen, A. Hamnett, G.L. Troughton, J. Electroanal. Chem. 362 (1993) 207.
[9] L. Liu, G. Pu, R. Viswanathan, Q.B. Fan, R.X. Liu, E.S. Smotkin, Electrochim. Acta 43 (1998) 3657.
[10] S. Wasmus, A. Küver, J. Electroanal. Chem. 461 (1999) 14.
[11] M. Uchida, Y. Fukuoka, Y. Sugawara, N. Eda, A. Ohta, J. Electrochem. Soc. 143 (1996) 245.
[12] M. Uchida, Y. Fukuoka, Y. Sugawara, H. Ohara, A. Ohta, J. Electrochem. Soc. 145 (1998) 3708.
[13] C.A. Bessel, K. Laubernds, N.M. Rodriguez, R.T.K. Baker, J. Phys. Chem. B 105 (2001) 1115.
[14] E.S. Steigerwalt, G.A. Deluga, D.E. Cliffel, C.M. Lukehart, J. Phys Chem B 105 (2001) 8097.
[15] D.L. Boxall, G.A. Deluga, E.A. Kenik, W.D. King, C.M. Lukehart, Chem. Mater. 13 (2001) 891.
[16] E.S. Steigerwalt, G.A. Deluga, C.M. Lukehart, J. Phys. Chem. B 106 (2002) 760.
[17] C. Wang, M. Waje, X. Wang, J.M. Tang, R.C. Haddon, Y. Yan, Nano Lett. 4 (2004) 345.
[18] Z. He, J. Chen, D. Liu, H. Tang, W. Deng, Y. Kuang, Mater. Chem. Phys. 85 (2004) 396–401.
[19] C.L.W. Li, J. Qiu, W. Zhou, H. Han, Z. Wei, G. Sun, Q. Xin, Carbon 40 (2002) 787–803.
[20] G. Che, B.B. Lakshmi, C.R. Martin, E.R. Fisher, Langmuir 15 (1999) 750.
[21] T. Hyeon, S. Han, Y.E. Sung, K.W. Park, Y.W. Kim, Angew. Chem. Int. Ed. 42 (2003) 4352–4356.
[22] K.W. Park, Y.E. Sung, S. Han, Y. Yun, T. Hyeon, J. Phys. Chem. B 108 (2004) 939.
[23] G.S. Chai, S.B. Yoon, J.S. Yu, J.H. Choi, Y.E. Sung, J. Phys. Chem. B 108 (2004) 7074.
[24] S.H. Joo, S.J. Choi, I. Oh, J. Kwak, Z. Liu, O. Terasaki, R. Ryoo, Nature 412 (2001) 169.
[25] Y. Takasu, T. Kawaguchi, W. Sugimoto, Y. Murakami, Electrochim. Acta 48 (2003) 3861.
[26] A.S. Arico, L. Pino, P.L. Antonucci, N. Giordano, Carbon 28 (1990) 599.
[27] P.A. Simonov, V.A. Likholobov, in: A. Wieckowski, E.R. Savinova, C.G. Vayenas (Eds.), Catalysis and Electrocatalysis at Nanoparticle Surfaces, Marcel Dekker, New York, 2003, p. 409.
[28] Y.I. Yermakov, V.F. Surovikin, G.V. Plaksin, V.A. Semikolenov, V.A. Likholobov, A.L. Chuvilin, S.V. Bogdanov, React. Kinet. Catal. Lett. 33 (1987) 435.
[29] J.B. Donnet, R.C. Bansal, M.J. Wang, Carbon Blacks, Marcel Dekker, New York, 1993.
[30] Y. Takasu, H. Itaya, T. Iwazaki, R. Miyoshi, T. Ohnuma, W. Sugimoto, Y. Murakami, Chem. Commun. (2001) 341.
[31] K.A. Friedrich, K.P. Geyzers, A.J. Dickinson, U. Stimming, J. Electroanal. Chem. 524-525 (2002) 261.
[32] S. Guerin, B.E. Hayden, C.E. Lee, C. Mormiche, J.R. Owen, A.E. Russell, J. Comb. Chem. 6 (2004) 149.
[33] A.A. Kulikovsky, Electrochem. Commun. 5 (2003) 530–538.
[34] V. Gogel, T. Frey, Z. Yongsheng, K.A. Friedrich, L. Jörissen, J. Garche, J. Power Sources 127 (2004) 172–180.
[35] A. Havranek, K. Wippermann, J. Electroanal. Chem. 567 (2004) 305–315.
[36] M.T. Reetz, M.G. Koch, J. Am. Chem. Soc. 121 (1999) 7933.
[37] A.P. Karnaukhov, V.B. Fenelonov, V.Y. Gavrilov, Pure Appl. Chem. 61 (1989) 1913.
[38] E.P. Barrett, L.G. Joyner, P.P. Halenda, J. Am. Chem. Soc. 73 (1951) 373.
[39] A.L. Vishnevskii, V.V. Molchanov, T.A. Kriger, L.M. Plyasova, in International Conference on Powder Diffraction and Crystal Chemistry, St. Petersburg, 1994, p. 206.
[40] A. Guerrero-Ruiz, P. Badenes, I. Rodríguez-Ramos, Appl. Catal. A: Gen. 173 (1998) 313.
[41] F. Rodríguez-Reinoso, I. Rodríguez-Ramos, C. Moreno-Castilla, A. Guerrero-Ruiz, J.D. López-González, J. Catal. 99 (1986) 171.
[42] J.W. Long, R.M. Stroud, K.E. Swider-Lyons, D.R. Rolison, J. Phys. Chem. B 104 (2000) 9772.
[43] D.R. Rolison, P.L. Hagans, K.E. Swider, J.W. Long, Langmuir 15 (1999) 774.
[44] I.G. Batyev, A.N. Karavanov, Surface (Russian ed) 12 (1992) 83.
[45] J.F. Long, R.M. Stroud, K.E. Swider-Lyons, D.R. Rolison, J. Phys. Chem. B 104 (2000) 9772.
[46] E. Antolini, L. Giorgi, A. Pozio, E. Passalacqua, J. Power Sources 77 (1999) 136.
[47] G. Sasikumar, J.W. Ihm, H. Ryu, J. Power Sources 132 (2004) 11–17.
[48] A.S. Arico, A.K. Shukla, K.M. El-Khatib, P. Creti, V. Antonucci, J. Appl. Electrochem. 29 (1999) 671.
[49] A.S. Arico, P. Creti, P.L. Antonucci, J. Cho, H. Kim, V. Antonucci, Electrochim. Acta 43 (1998) 3719.
[50] H.N. Dinh, X. Ren, F.H. Garzon, P. Zelenay, S. Gottesfeld, J. Electroanal. Chem. 491 (2000) 222–233.
[51] T.R. Ralph, M.P. Hogarth, Platinum Met. Rev. 46 (2002) 3.
[52] Z. Jusys, T.J. Schmidt, L. Dubau, K. Lasch, L. Jörissen, J. Garche, R.J. Behm, J. Power Sources 105 (2002) 297.
[53] Z. Jusys, J. Kaiser, R.J. Behm, Electrochim. Acta 47 (2002) 3693.